International Journal of Heat and Mass Transfer 79 (2014) 24–33

Contents lists available at ScienceDirect

International Journal of Heat and Mass Transfer

journal homepage: www.elsevier.com/locate/ijhmt

Transient analysis of subcritical/supercritical carbon dioxide based natural circulation loops with end heat exchangers: Numerical studies

Ajay Kumar Yadav [a], M. Ram Gopal [b], Souvik Bhattacharyya [b,*]

[a] Department of Mechanical Engineering, National Institute of Technology Karnataka, Surathkal, Mangalore 575 025, India
[b] Department of Mechanical Engineering, Indian Institute of Technology Kharagpur, Kharagpur 721302, India

ARTICLE INFO

Article history:
Received 27 March 2014
Received in revised form 3 July 2014
Accepted 23 July 2014

Keywords:
Natural circulation loop
CFD
Turbulent flow
Supercritical carbon dioxide

ABSTRACT

Transient analysis of carbon dioxide based natural circulation loop (NCL) with end heat exchangers has been carried out. Subcritical and supercritical phases of CO_2 are considered with operating pressures in the range of 50–100 bar for an operating temperature range of 323 K to 363 K. Studies are carried out for various loop tilt angles, different initial conditions, and different water mass flow rates.

Results are obtained for various inlet temperatures of water in the hot heat exchanger while keeping the inlet temperature of cooling water in the cold heat exchanger fixed. Effect of tilting the loop in *XY* and *YZ* planes on transient as well as steady state behaviour of loop are also studied. Validation of simulation results against experimental and numerical results reported in the literature in terms of modified Grashof number (Gr_m) and Reynolds number (Re) show good agreement.

1. Introduction

In recent years, a growing popularity of carbon dioxide as secondary fluid has been witnessed in forced as well as natural circulation loops [1–3]. This may be attributed to the favourable thermo-physical properties of CO_2 in addition to its environment friendliness. Studies show that any fluid operating near its critical point offers thermophysical properties that are favourable to natural circulation loops (NCLs). Operating temperatures of many engineering applications lie around the critical temperature of CO_2 (31.2 °C), which makes CO_2 one of the best working fluids for NCLs. However, high critical pressure of CO_2 (73.8 bar) is one of the demerits. NCLs offer certain advantages over forced circulation loops, particularly in small to medium capacity systems; they are preferred where safety is of foremost concern, for example, in nuclear power plants. NCLs are also widely used in applications such as refrigeration and air conditioning systems, solar collectors, and nuclear reactors. Studies show that for low temperature refrigeration and air conditioning applications, use of CO_2 in place of conventional secondary fluids results in very compact loops [2]. CO_2 based NCLs have also been proposed for various heat transfer applications such as new generation nuclear reactors [4], in chemical extraction [5,6], cryogenic refrigeration [7], heat pump [8], electronic cooling systems [9], geothermal applications [10,11], etc. However, detailed modelling and analyses of CO_2 based NCLs are relatively sparse in the literature. Kiran Kumar and Ram Gopal [12] reported a one-dimensional steady-state analysis of a rectangular NCL with end heat exchangers for low temperature applications. Recently Zhang et al. [13] and Chen et al. [14] reported studies on the effects of heat transfer and the instabilities of supercritical CO_2 flow in a 2-D NCL at a fixed operating pressure of 90 bar operating over a large heat source temperature range. It was concluded that using supercritical CO_2 as the loop fluid, a temperature difference as small as 25 K between heating and cooling sources can yield a Reynolds number as high as 6×10^4, resulting in high heat transfer rates. Most of the studies available for CO_2 based NCLs are for isothermal heat source and sink, which has less practical significance than NCLs with end heat exchangers.

In addition, to account for the strong local buoyancy effects near pseudo critical zone, and the effect of bends in pipe, etc., it becomes essential to consider a three-dimensional (3-D) model for greater accuracy. Recently, Yadav et al. [15,16] have reported a three-dimensional steady state analysis on CO_2 based NCLs. Review of literature shows that transient analysis of CO_2 based NCLs employing 3-D models are not available in the open literature. To fill in that void, this study presents a CFD analysis of a three-dimensional model of subcritical/supercritical CO_2 based NCL with end heat exchangers. Results are presented on the transient behaviour of the loop at various operating pressures and temperatures. The operating parameter range is chosen such that the loop fluid (CO_2) exists as a subcritical or supercritical single-phase fluid.

* Corresponding author. Tel.: +91 3222282904; fax: +91 3222282278.
E-mail address: souvik.iit@gmail.com (S. Bhattacharyya).

http://dx.doi.org/10.1016/j.ijheatmasstransfer.2014.07.068
0017-9310/

Nomenclature

A	area
C_μ $C_{1\varepsilon}$ $C_{2\varepsilon}$ $C_{3\varepsilon}$	parameters in RNG model equations
c_p	specific heat capacity
C_v	constant
D	diameter of outer pipe of CHX and HHX
d	diameter of inner pipe or loop diameter
E	energy
f	friction factor
g	gravitational acceleration
G_b	turbulent kinetic energy due to buoyancy
G_k	turbulent kinetic energy due to mean velocity gradient
Gr	Grashof number
Gr_m	modified Grashof number
h	heat transfer coefficient
H_0	total height of vertical pipes
k	turbulent kinetic energy
L	length of CHX (sink) and HHX (source)
L_0	total length of a horizontal pipe
L_1	adiabatic pipe length on horizontal pipe
L_c	characteristic length
L_t	total length of the loop
m	mass flow rate
Nu	Nusselt number
p P	pressure of fluid
Pr	Prandtl number
Pr_t	turbulent Prandtl number
Q	heat transfer rate
r	radius of loop
R	radius of curvature for bends
Ra	Rayleigh number
Re	Reynolds number
R_ε	parameters in RNG model equations
S	strain tensor
T	temperature
t	time
u v V	velocity
x	x-coordinate location

Greek letters

α α_0	thermal diffusivity
α_k α_ε	parameters in RNG model equations
β	volumetric expansion coefficient
ΔT	temperature difference across the CHX/HHX
ε	turbulence dissipation rate
λ	thermal conductivity
μ	dynamic viscosity
μ_t μ_{eff}	viscosity parameters in RNG model
η	parameter in RNG model
ρ	density of fluid
$\bar{\bar{\tau}}$	stress tensor

Subscripts

avg	average
c	critical
C	cold heat exchanger, sink
CO_2	carbon dioxide
eff	effective
f	fluid
H	hot heat exchanger, source
i	x-direction/internal
j	y-direction
m	modified, bulk mean
max	maximum
o	external
ref	reference
r	radial direction
s	pseudocritical/optimum/solid
θ	azimuthal direction
w	water, wall
z	axial direction

2. Physical model and mathematical formulations

2.1. Physical model

A three dimensional geometry shown in Fig. 1a is prepared in ANSYS 14.0 using Design Modeler. Figure shows the schematic of a rectangular NCL comprising a cold heat exchanger (CHX), a hot heat exchanger (HHX), a riser and a downcomer. The loop fluid is heated sensibly by extracting heat from the external fluid (hot water) in HHX and is cooled sensibly by rejecting heat to the external fluid (cold water) in the CHX. Circulation of the loop fluid is maintained due to the buoyancy effect caused by heating at the bottom and cooling at the top. Flow in the clockwise direction is considered positive. Based on commercial availability of stainless steel and copper tubes, diameter of the pipes are chosen for the simulation and the entire geometric and material specification of the model is listed in Table 1.

Studies are carried out at different tilt angles of the loop in *XY* and *YZ* planes. Fig. 1b shows the rotation of the loop in *XY* plane in clockwise direction. The loop is considered to be vertical at a tilt angle of 0°. The loop is also tilted in the *YZ* plane from vertical position in counter clockwise direction as depicted in Fig. 1c. During simulation, most of the transient analysis results have been taken at the cross section in the middle of the left leg pipe.

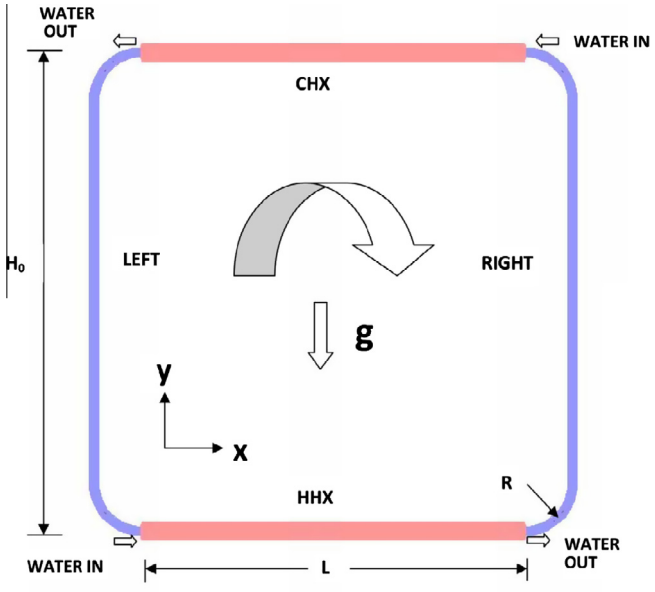

Fig. 1a. Schematic of the NCL with end heat exchangers.

Table 1
Geometric and material specifications for the model.

Parameter	Value
HHX and CHX	
Inner tube inner diameter (SS)	7.3 mm
Inner tube outer diameter (SS)	9.6 mm
Outer tube inner diameter (Cu)	16 mm
Outer tube outer diameter (Cu)	19.2 mm
Length of heat exchangers (L)	390 mm
Height of the loop (H_0)	500 mm
Width of the loop (L_0)	500 mm
Internal diameter of the loop	7.3 mm
Curvature radius of the bend (R)	50 mm
Total length of the loop (L_t)	1914 mm
Material of the loop	SS

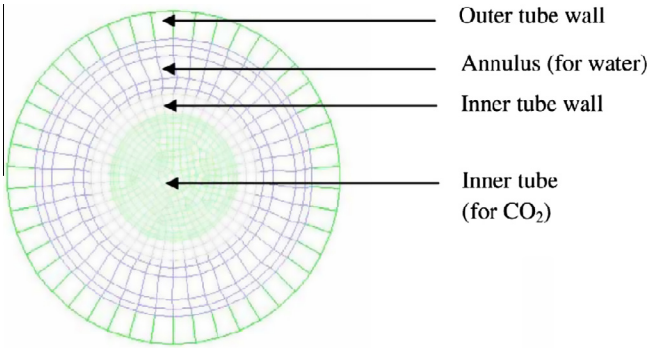

Fig. 2. Meshing of a cross section at CHX/HHX.

2.2. Grid generation

Meshing of a three dimensional geometry is carried out in ANSYS 14.0 and Fig. 2 illustrates a sample meshing of a cross section of the loop at CHX/HHX. Uniform surface meshing is carried out for the thickness of walls. For the CO_2 side, a minimum grid size of 0.2 mm is considered in the radial direction near the wall which increased to the maximum grid size of 0.5 mm away from the wall. For the water side, a minimum grid size of 0.4 mm is taken in the radial direction near the wall, increasing to the maximum grid size of 1.0 mm away from the wall. Coarse meshing is adopted in the axial direction (5 mm grid size in horizontal pipes including bends and 10 mm for vertical insulated pipes). This strategy of mesh generation yielded a total of 210,292 nodes. Maximum skewness of the meshing is 0.421. The value of nondimensional parameters Y^+ and Y^* are checked for all the cases of turbulent flow to ensure optimal choice of fineness of grid. Maximum Y^+ and Y^* values in the present study are 49.0 and 72.1, respectively, which ensures that the grid is suitable for the assumption of standard wall function near the wall [17]. Parameters Y^+ and Y^* are defined as:

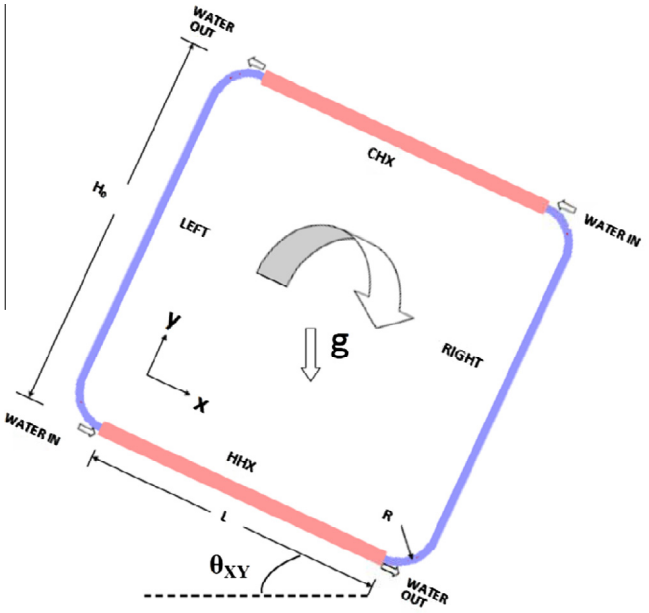

Fig. 1b. Rotation of the loop in *XY* plane (front view).

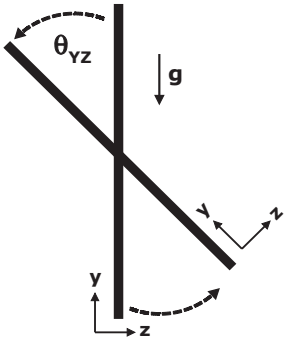

Fig. 1c. Rotation of the loop in *YZ* plane (side view).

$$Y^+ \equiv \rho u_\tau y/\mu \tag{1}$$

where, u_τ is the friction velocity, defined as $\sqrt{(\tau_w/\rho)}$, in which τ_w is the wall shear stress.

$$Y^* \equiv \frac{\rho C_\mu^{1/4} k^{1/2} y}{\mu} \tag{2}$$

where, k = turbulent kinetic energy, y = distance from the wall, C_μ = 0.0845.

Grid independence tests were carried out and results with fine and coarse grids were compared (Table 2). In case of fine grid, 0.1 mm grid size is considered near the wall and 0.4 mm away from the wall; for coarse grid, a 0.3 mm grid size is considered near the wall and 0.6 mm away from the wall. Results are obtained for loop operating pressure of 90 bar with HHX and CHX water inlet temperature of 363 K and 305 K respectively. Performance of the loop is presented in terms of mass flow rate (m) and heat transfer rate (Q). Differences in results compared with fine grid are less than 2% for the present study.

2.3. Mathematical formulation and solution methodology

The standard conservation equations are shown below. These equations with relevant boundary conditions are solved by the commercial software, ANSYS (FLUENT) 14.0.

Conservation of mass is given by:

$$\frac{\partial \rho}{\partial t} + \nabla \cdot (\rho \vec{V}) = 0 \tag{3}$$

Conservation of momentum is expresses as:

$$\frac{\partial (\rho \vec{V})}{\partial t} + \nabla \cdot (\rho \vec{V} \vec{V}) = -\nabla p + \nabla \cdot \left(\bar{\bar{\tau}}\right) + \rho \vec{g} \tag{4}$$

Table 2
Grid independence test results.

90 bar	Grid size in radial direction for CO_2 (mm)		
T_C = 305 K T_H = 363 K	Min. size: 0.1 mm Max. size: 0.4 mm (fine grid)	Min. size: 0.2 mm Max. size: 0.5 mm (present study)	Min. size: 0.3 mm Max. size: 0.6 mm (coarse grid)
m (kg/s) Q (W)	0.00476 128	0.00481 130	0.00474 126

where the stress tensor can be written as:

$$\overline{\overline{\tau}} = \mu\left[\left(\nabla\vec{V} + \nabla\vec{V}^{T}\right) - \frac{2}{3}\nabla\cdot\vec{V}I\right]$$

The second term in stress tensor is the effect of volume dilation, and I is the unit tensor.

Conservation of energy with viscous dissipation may be expressed as:

$$\frac{\partial(\rho E)}{\partial t} + \nabla\cdot(\vec{V}(\rho E + p)) = \nabla\cdot\left(\lambda_{eff}\nabla T + \overline{\overline{\tau}}\cdot\vec{V}\right) \quad (5)$$

where,

$$E = \int_{T_{ref}}^{T} c_p dT + \frac{V^2}{2} \quad (6)$$

and, T_{ref} = 298.15 K.

2.3.1. Model for turbulence analysis

Turbulent models for supercritical fluids are less developed and still under intense study [18]. Therefore, in the present simulation, a general *Renormalization Group* (RNG) $k-\varepsilon$ model is employed to introduce the expression of turbulent effect. This method has also been used successfully in previous studies on supercritical CO_2 turbulent flow yielding accurate results [19,20].

The transport equations for RNG k–ε model are written as:

$$\frac{\partial}{\partial t}(\rho k) + \frac{\partial}{\partial x_i}(\rho k u_i) = \frac{\partial}{\partial x_j}\left(\alpha_k \mu_{eff}\frac{\partial k}{\partial x_j}\right) + G_k + G_b - \rho\varepsilon \quad (7)$$

$$\frac{\partial}{\partial t}(\rho\varepsilon) + \frac{\partial}{\partial x_i}(\rho\varepsilon u_i) = \frac{\partial}{\partial x_j}\left(\alpha_\varepsilon \mu_{eff}\frac{\partial \varepsilon}{\partial x_j}\right) + C_{1\varepsilon}\frac{\varepsilon}{k}(G_k + C_{3\varepsilon}G_b) - C_{2\varepsilon}\rho\frac{\varepsilon^2}{k} - R_\varepsilon \quad (8)$$

where G_k and G_b are the generation of turbulence kinetic energy due to the mean velocity gradients and buoyancy, respectively:

$$G_k = \mu_t S^2 \quad (9)$$

where S is the modulus of the mean rate-of-strain tensor, defines as

$$S \equiv \sqrt{2S_{ij}S_{ij}} \quad (10)$$

S_{ij} is the rate-of-strain tensor defined as,

$$S_{ij} \equiv \frac{1}{2}\left(\frac{\partial u_i}{\partial x_i} + \frac{\partial u_j}{\partial x_i}\right) \quad (11)$$

$$\mu_t = \rho C_\mu k^2/\varepsilon \quad (12)$$

Generation of turbulence due to buoyancy is given by:

$$G_b = \beta g_i \frac{\mu_t}{\mathrm{Pr}_t}\frac{\partial T}{\partial x_i} \quad (13)$$

$$\text{where,}\quad \beta = -\frac{1}{\rho}\left(\frac{\partial\rho}{\partial T}\right)_p \quad (14)$$

$$Pr_t = 1/\alpha \quad (15)$$

$$\left|\frac{\alpha - 1.3929}{\alpha_0 - 1.3929}\right|^{0.6321}\left|\frac{\alpha + 2.3929}{\alpha_0 + 2.3929}\right|^{0.3679} = \frac{\mu}{\mu_{eff}} \quad (16)$$

$$\alpha_0 = 1/Pr = \lambda/\mu c_p \quad (17)$$

$$R_\varepsilon = \frac{C_\mu\rho\eta^3(1-\eta/\eta_0)\varepsilon^2}{(1+0.012\eta^3)k} \quad (18)$$

where, $\eta \equiv Sk/\varepsilon$; η_0 = 4.38; C_μ = 0.0845; $\alpha_k = \alpha_\varepsilon$ = 1.393; $C_{1\varepsilon}$ = 1.42; $C_{2\varepsilon}$ = 1.68;

$$C_{3\varepsilon} = \tanh\left|\frac{v}{u}\right| \quad (19)$$

v is the component of the flow velocity parallel to the gravitational vector and u is the component of the flow velocity perpendicular to the gravitational vector.

Equation for the effective viscosity is given by:

$$d\left(\frac{\rho^2 k}{\sqrt{\varepsilon\mu}}\right) = 1.72\frac{\hat{\nu}}{\sqrt{\hat{\nu}^3 - 1 + C_\nu}}d\hat{\nu} \quad (20)$$

$$\text{where,}\quad \hat{\nu} = \mu_{eff}/\mu \quad (21)$$

and, $C_\nu \approx 100$

Effective conductivity is expressed as,

$$\lambda_{eff} = \alpha C_p \mu_{eff} \quad (22)$$

The following terms are defined to describe the fluid flow and heat transfer phenomena.

Mass flow rate at any cross section is defined as,

$$m = \int_0^A \rho V dA \quad (23)$$

Local bulk mean temperature of the fluid is expressed as,

$$T = \frac{\int_0^A c_p T\rho V dA}{\int_0^A c_p \rho V dA} \quad (24)$$

Steady-state Reynolds number and modified Grashof number [21] are defined as,

$$Re = \frac{4m}{\pi d\mu} \quad (25)$$

$$Gr_m = \frac{g\beta d^3\rho^2 Q H_0}{A\mu^3 c_p} \quad (26)$$

where, Q is the heat transfer rate from heat source to the sink.

Prandtl number is defined as,

$$Pr = \frac{\mu c_p}{\lambda} \quad (27)$$

Nusselt number is defined as,

$$Nu = \frac{\bar{h}d}{\lambda} \quad (28)$$

where $\bar{h}$ is the area weighted average wall function heat transfer coefficient:

$$\bar{h} = \frac{\int_0^A h dA}{\int_0^A dA} \tag{29}$$

$$\text{Heat transfer rate,} \quad Q = -\int_0^A \left(\lambda \frac{\partial T}{\partial r}\right) dA = \int_0^A h(T_s - T_f) dA, \quad at\ r = r_i \tag{30}$$

where T_s and T_f are the solid wall temperature and bulk mean fluid temperature at a cross section, respectively.

Friction factor is defined as,

$$f = \frac{\pi^2 \rho \Delta p d^5}{8 m^2 L} \tag{31}$$

where Δp is the total pressure drop in the pipe of length L.

All the properties are calculated at the bulk mean temperature (T_m) of loop fluid, defined as:

$$T_m = \frac{\sum_{i=1}^{n} T_i}{n} \tag{32}$$

where n is the number of cross sections considered in the loop.

Average temperature of the loop is defined as,

$$T_{avg} = \frac{T_C + T_H}{2} \tag{33}$$

where T_C and T_H are the water inlet temperature at the cold and hot heat exchanger respectively.

For wall conduction, the governing equation is expressed as:

$$\nabla^2 T + \frac{1}{\alpha_w} \frac{\partial T}{\partial t} = 0 \tag{34}$$

where α_w is thermal diffusivity of the wall.

The modified Grashof number expressed in Eq. (26) is somewhat different from the classical Grashof number. Bau and Torrance [22] prefer to call it a non-dimensional heating rate. However, as the term $QH/(A\mu c_p)$ has the dimensions of temperature difference and if we consider it as the reference temperature difference, then it is appropriate to refer to it as a *modified Grashof number* [21] as reported lately [13,20,23,24] in the study of NCLs.

Boundary conditions:

(i) No-slip and no-penetration boundary conditions are applied near the walls.
(ii) All external walls are perfectly insulated.
(iii) For internal walls conjugate heat transfer is considered.
(iv) Water inlet temperature at cold and hot heat exchangers is known.

2.3.2. Simulation details

The governing mass, momentum and energy equations are solved employing the CFD code, ANSYS (FLUENT) 14.0. A 3-D geometry was prepared in ANSYS 14.0 2.4.6 and transient simulation was carried out, where the implicit-coupled finite-volume method was used to discretize the governing equations. The *pressure-implicit with splitting of operators* (PISO) algorithm was used to solve the coupling model between velocity and pressure.

The momentum and energy terms in the governing equations are iterated with a second-order upwind scheme that uses the upstream values and gradients to compute the control volume parameters. Turbulence parameters (k, ε, etc.) are also iterated with a second-order upwind scheme. The PRESTO (*Pressure Staggering Option*) scheme is used to discretize the pressure term. A general *Renormalization Group* (RNG) $k-\varepsilon$ model is selected as the first step to introduce the expression of turbulent effect. For the near wall treatment, a standard wall function has been assumed in case of turbulent flow [17]. Axial conduction and viscous dissipation in fluid are considered, while axial conduction along the tube wall is incorporated as well. Convergence is obtained when various residuals of the parameters (temperature, velocity, pressure, etc.) change with the iterations within a preset convergence criterion of 10^{-3} for the residuals of continuity equation and 10^{-6} for the energy equation. Conservation of mass and energy are also checked for all the cases in the analysis. A very small time step of the order of 10^{-4} was adopted to attain convergence during the numerical simulation which was carried out in a configured computer with an i5 processor and 4 GB RAM. Average computational time to obtain each simulation result was 20 days.

2.4. Calculation of thermo-physical properties of CO_2 and water

Since the state of CO_2 inside the loop varies from subcritical to supercritical and the variation in thermo-physical properties near the critical point is extremely large, it is essential to adequately capture the property variation due to changes in temperature. However, as shown in the literature, due to very small variation in operating pressure throughout the NCL the effect of variation of pressure on the properties of single phase CO_2 is not expected to be significant [12,13]. Hence, the properties of CO_2 at any point in the loop are calculated at the fixed operating pressure and local temperature. The required properties of CO_2 including density, specific heat, thermal conductivity and viscosity are obtained from the NIST Standard Reference Database REFPROP version 8 (2006). Properties of CO_2 for the operating temperature range at a temperature difference of 1 K are added to the fluid properties library, and a piecewise-linear interpolation approach is used to calculate the properties within 1 K temperature difference. Fig. 3 shows the comparison of specific heat data used in FLUENT for this study with REFPROP data. Maximum variation with temperature is observed in case of specific heat (c_p), while for the remaining thermo-physical properties (density, thermal conductivity and viscosity) the regression correlation coefficient is good.

Properties of water are taken at the inlet temperature of heat exchanger and are considered to remain constant throughout the heat exchanger, due to small variation in water temperature (3 K) in the heat exchanger.

3. Results and discussion

Mass flow rate of water in CHX as well as in HHX was assumed to remain constant at a value of 0.05 kg/s except where it is

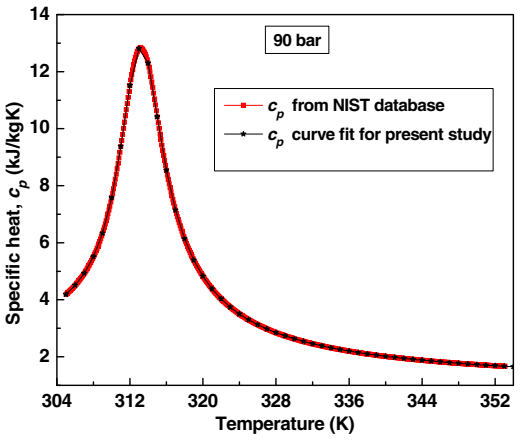

Fig. 3. Curve fit data for specific heat of supercritical CO_2.

mentioned, which ensures turbulent flow on water side. Operating pressure of the loop is defined at the centre of inlet to the HHX. Initial temperature of the loop is taken as 305 K before the start of simulation. It may be noted that most of the transient analysis results have been plotted at the centre of left leg.

3.1. Effect of hot water inlet temperature

Figs. 4a–4c show the effect of hot water inlet temperature on mass flow rate, temperature and axial velocity of CO_2, respectively. The left leg centre is the spatial location where all the flow parameters are estimated. Average temperature of the loop at a hot water inlet temperature of 323 K is close to the pseudo-critical region for a pressure of 90 bar. Near the pseudo-critical region, there is a very large variation of thermo-physical properties leading to fluctuation or instability in the beginning of flow. Since the loop is geometrically symmetrical, and thermally almost symmetrical (in/out temperature difference of heat exchanger is less than 1 K), the chances of flow reversal is greater. Results show that flow direction of the loop fluid gets reversed at 323 K due to initial instability of flow as well as due to symmetry of the loop. Figures also show that loop mass flow rate reaches steady state faster compared to temperature. Hence, as a conservative estimate, the time for the system to reach steady state should be obtained from the variation in temperature instead of the mass flow rate. Fig. 4b shows that even though there is initial fluctuation at 323 K, time to reach steady state is almost the same.

Fig. 4d shows the effect of hot water inlet temperature on the heat transfer and mass flow rate of CO_2. Due to the excellent thermo-physical properties near pseudo-critical temperature, mass flow rate at 323 K is found to be the maximum leading to high heat transfer coefficient (shown in Table 3). Heat transfer rate increases with increase in hot water inlet temperature which is caused by the higher temperature difference between CHX and HHX. But mass flow rate of loop fluid does not increase at higher temperature due to its lower density at higher temperature. Table 3 shows that the CO_2 side heat transfer coefficient near pseudo-critical point (T_H = 323 K) is higher and close to water side heat transfer coefficient which implies lower irreversibility in heat exchangers. This also implies that the operating condition of loop fluid (CO_2) should be close to the pseudo-critical region.

3.2. Effect of operating pressure

Figs. 5a–5c show the effect of operating pressure on mass flow rate and temperature (tilt angle of 0° & 15°) of CO_2 for a hot water inlet temperature of 323 K. Results were obtained at left leg centre for operating pressure within the range of 50–100 bar. At this operating temperature, an operating pressure of 90 bar is closer to the pseudo-critical point. Trends show that amplitude of fluctuation is quite large at 90 bar compared to other operating pressures. This

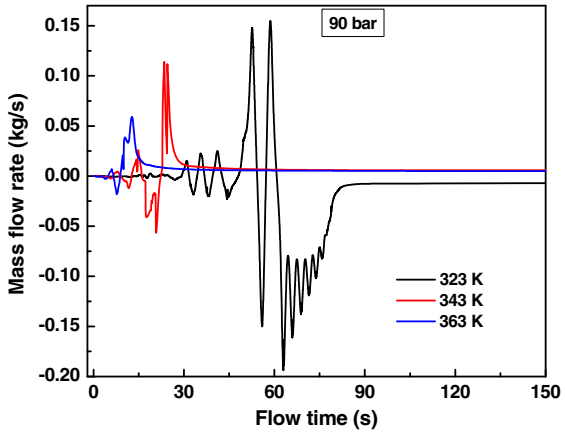

Fig. 4a. Effect of hot water inlet temperature on mass flow rate of CO_2.

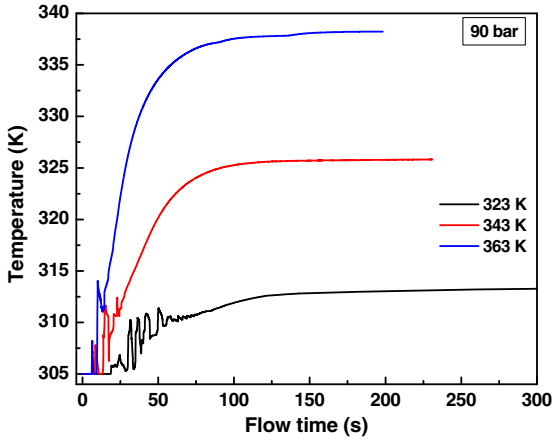

Fig. 4b. Effect of hot water inlet temperature on the temperature of CO_2 at left leg centre.

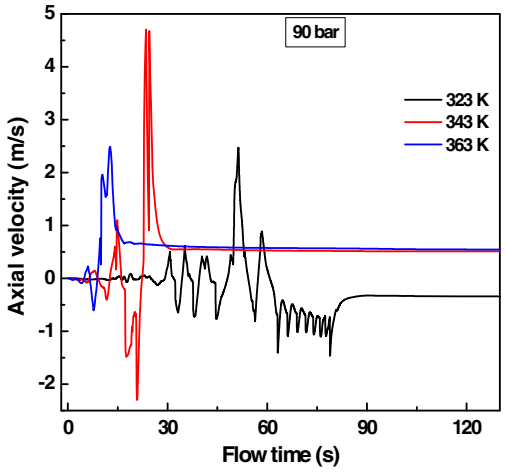

Fig. 4c. Effect of hot water inlet temperature on the axial velocity of CO_2.

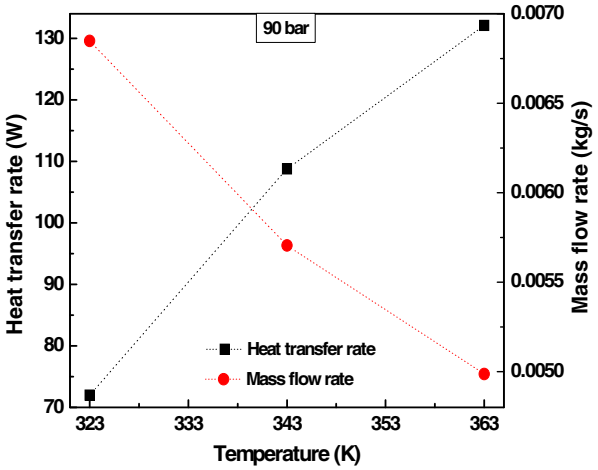

Fig. 4d. Effect of hot water inlet temperature on the heat transfer and mass flow rate of CO_2.

Table 3
Heat transfer coefficient on CO_2 side and water side at 90 bar.

T_H (K)	Heat transfer coefficient on CO_2 side (W/m^2 K)		Heat transfer coefficient on water side (W/m^2 K)	
	CHX	HHX	CHX	HHX
323	2530	2331	3055	3271
343	1394	1101	3056	3773
363	1016	817	3057	4239

could be attributed to the large variation of properties near pseudo-critical point as explained above. Due to initial fluctuation in flow, time required to reach steady state increases. To reduce fluctuation loop is tilted in *XY* plane by 15° and results are shown in Fig. 5c to see the effect of pressure on time to reach steady state at lesser intensity/frequency of fluctuation. At 90 bar, larger time is required to reach steady state at the tilt angle of 0° (Fig. 5b) due to higher degree of fluctuation. Figs. 5b and 5c show that the time required to reach steady state decreases as operating pressure increase provided initial fluctuation should be low. At constant temperature, all thermophysical properties (i.e., density, specific heat, volumetric expansion coefficient, viscosity) of CO_2 increase with increase in operating pressure. A higher value of thermophysical properties except viscosity is considered to be favourable for NCLs and these properties in combination lead the system to reach steady state faster. Table 4 show the time to reach steady state for different operating pressure and fixed HHX inlet temperature of 323 K at tilt angle of 15°. Results also reveal that mass flow rate

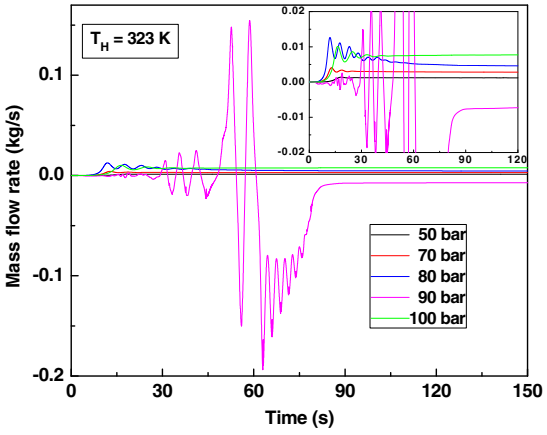

Fig. 5a. Effect of operating pressure on mass flow rate of CO_2.

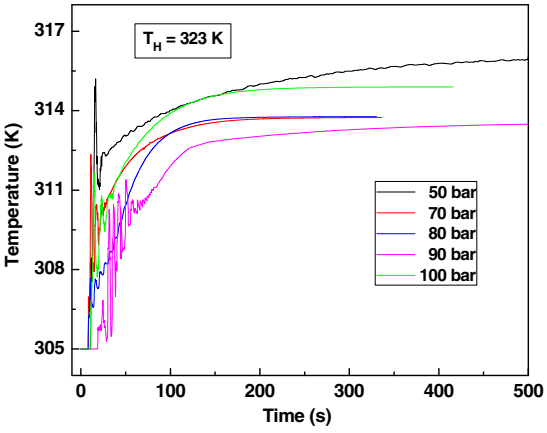

Fig. 5b. Effect of operating pressure on temperature of CO_2.

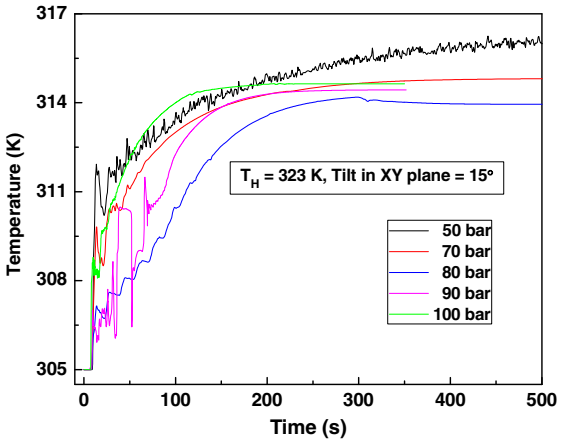

Fig. 5c. Effect of operating pressure on temperature of CO_2 at the tilt angle of 15°.

in case of 90 bar is higher than all other cases and again this may be attributed to the favourable thermo-physical properties near the pseudo-critical region.

3.3. Effect of tilt angle

Investigation was carried out on the effect of tilt angle variation on the system. Figs. 6a–6c exhibit how tilt angle influences mass flow rate, axial velocity and temperature of CO_2 respectively at 100 bar for a hot water inlet temperature of 333 K. The test loop was tilted in both *XY* and *YZ* planes to capture the effect of various inclinations. It may be observed that the system reaches steady state in the shortest time in case of the maximum tilt angle (45°). Results also show that for a zero tilt, amplitude of fluctuation is the maximum and it decreases as tilt angle increases. It can be also noted that the flow start-up time and fluctuation in flow parameters for tilt in *YZ* plane (45°) is higher than *XY* plane. Because tilting loop in *YZ* plane does not make any difference in symmetry of the loop, whereas tilting in *XY* plane makes a loop thermally and geometrically unsymmetrical which helps in reduction of fluctuation of flow parameters as well as the flow start-up time. Thus a more stable behaviour of the loop can be assured with a small angle of tilt of the loop in *XY* plane than in *YZ* plane.

Steady state results for mass flow rate and heat transfer rate are shown in Fig. 6d which exhibits deterioration in mass flow rate as well as heat transfer rate with increase in loop tilt angle in both the planes. It happens due to decrease in effective height of the loop which suppresses buoyancy effect. Differences in output parameters i.e., mass flow rate and heat transfer rate for *XY* and *YZ* planes are considered to be negligible till a tilt angle of 45°.

Table 4
Time to reach steady state for different operating pressure at tilt angle of 15°.

	50 bar	70 bar	80 bar	90 bar	100 bar
Time (s)	650	420	300	250	200

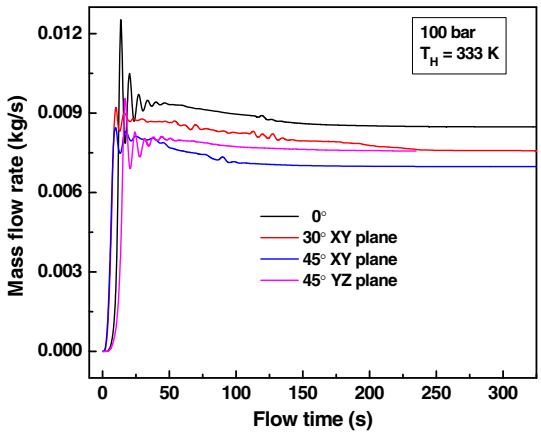

Fig. 6a. Effect of tilt angle on mass flow rate.

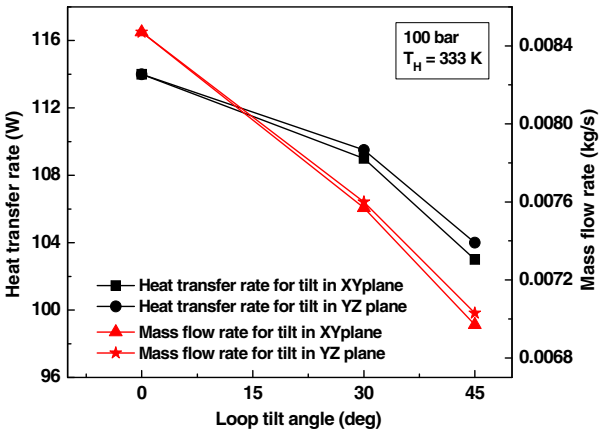

Fig. 6d. Effect of tilt angle on mass flow rate and heat transfer rate at steady state.

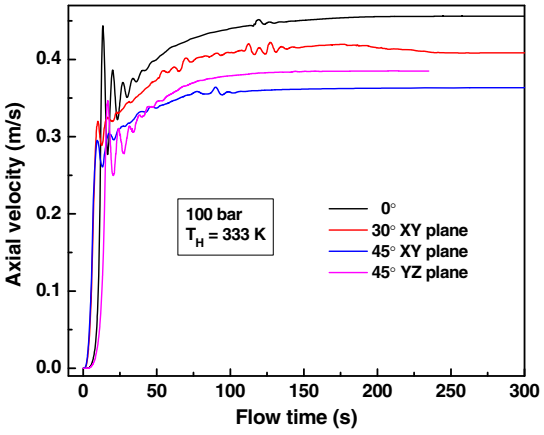

Fig. 6b. Effect of tilt angle on axial velocity.

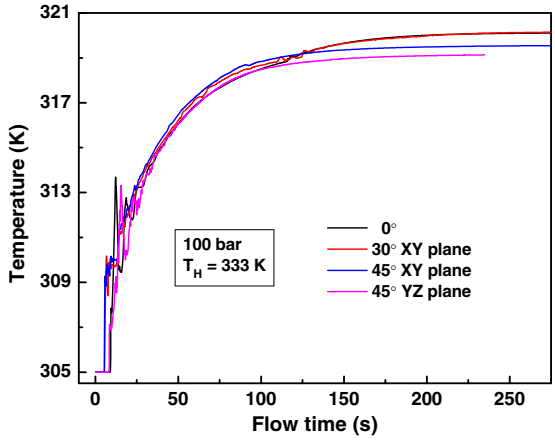

Fig. 6c. Effect of tilt angle on temperature.

3.4. Effect of Initial conditions

Studies were also conducted to explore how the initial condition affects the mass flow rate and temperature of CO_2. Figs. 7a and 7b present this aspect at 100 bar for a hot water inlet temperature of 333 K. As initial temperature of the loop increases, the system attains steady state sooner. This may be attributed to the fact that, as initial temperature increases, it approaches the final average temperature of the loop faster leading to an earlier attainment of steady state.

3.5. Effect of water mass flow rate

Water mass flow rate was observed to have a significant impact on mass flow rate and temperature of CO_2. Figs. 8a and 8b exhibit such effects at 100 bar for a hot water inlet temperature of 333 K with water mass flow rate at CHX and HHX kept identical for the simulation exercise. Trends show that increase in mass flow rate of water leads to an increase in mass flow rate of CO_2 as well.

Fig. 8c depicts the steady state heat transfer rate as well as mass flow rate of CO_2 at various water flow rates. The plots show heat transfer rate and mass flow rate of CO_2 to increase with increase in water mass flow rate. Transient results indicate that the system reaches steady state faster at larger mass flow rate of water which could be attributed to the higher heat transfer rate at such conditions.

3.6. Effect of disturbances on stability of the loop

A quantified measure on the influence of disturbances on loop stability was obtained through the simulation exercise; such results are of importance in many practical applications of critical nature. Fig. 9 shows such effects at 90 bar and at a hot water inlet temperature of 323 K. Since a greater degree of fluctuation and flow reversal was observed for this operating condition, it would be appropriate to study this operating condition for the proposed stability analysis. Stability of the loop was checked by stopping and starting the hot water and cold water pumps. Results indicate that the loop is stable for all the cases of perturbation applied.

3.7. Validation of obtained results

A validation exercise was undertaken for the results obtained from the CFD analysis. Comparisons were made against experimental data reported earlier by Vijayan [23] for a water based NCL and with numerical results reported earlier by Yadav et al. [16] for a CO_2 based NCL. Comparison is made in terms of non-dimensional parameters, namely, Reynolds number (Re) and modified Grashof number (Gr_m) calculated at the average temperature (T_{avg}) of the loop.

The Vijayan correlation [23] for turbulent flow (experimental) is expressed as,

$$Re = 1.96(Gr_m d/L_t)^{\frac{1}{2.75}} \quad (35)$$

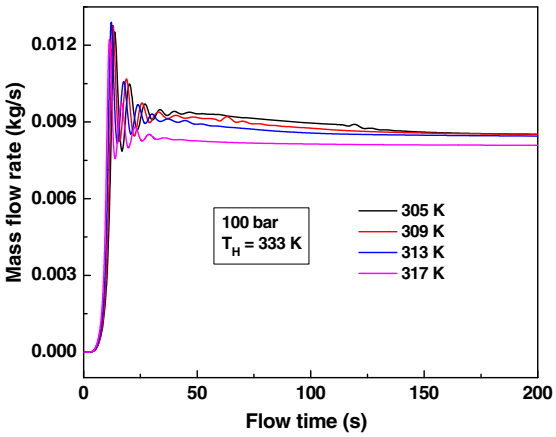

Fig. 7a. Effect of initial temperature of loop on mass flow rate.

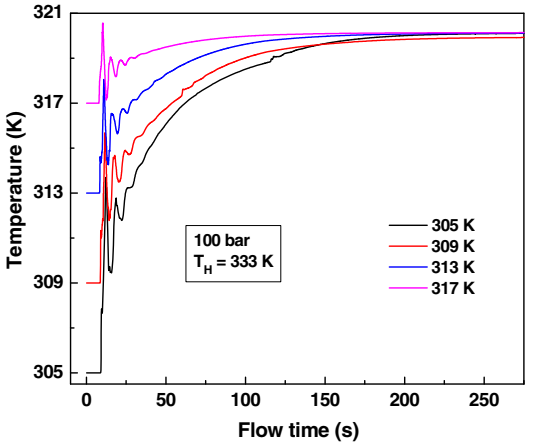

Fig. 7b. Effect of initial temperature of loop on temperature.

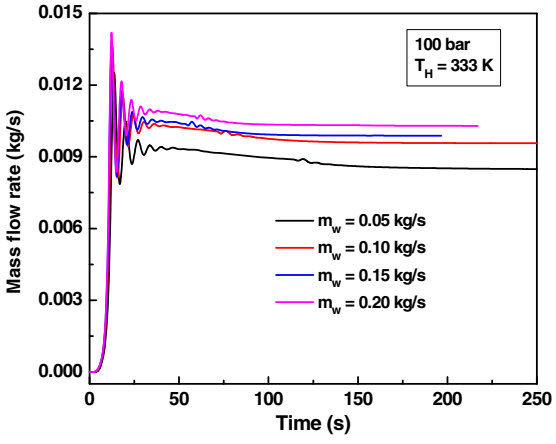

Fig. 8a. Effect of water mass flow rate on mass flow rate of CO_2.

The correlation given by Yadav et al. [16] for turbulent flow (numerical) is expressed as,

$$Re = 2.066(Gr_m d/L_t)^{\frac{1}{2.77}} \quad (36)$$

Fig. 10 shows that there is a good match in the trends between the presented data and the published experimental/numerical results although the absolute quantities differ, albeit quite modestly. Maximum difference between the simulation prediction

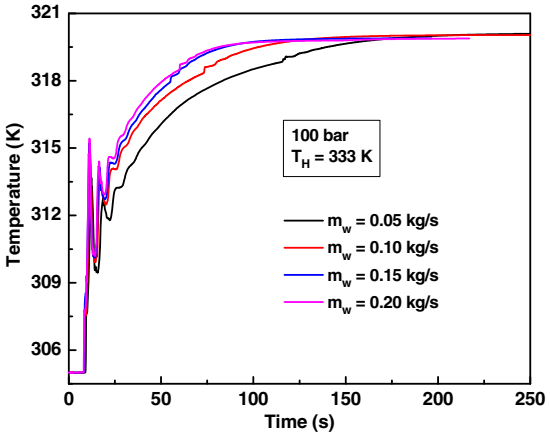

Fig. 8b. Effect of water mass flow rate on temperature of CO_2.

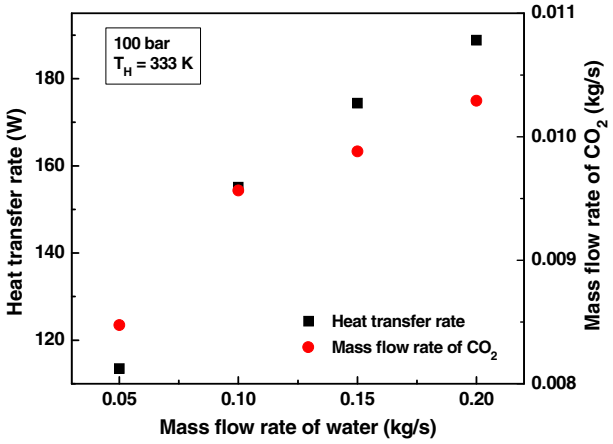

Fig. 8c. Effect of water mass flow rate on mass flow rate and heat transfer rate of CO_2 at steady state.

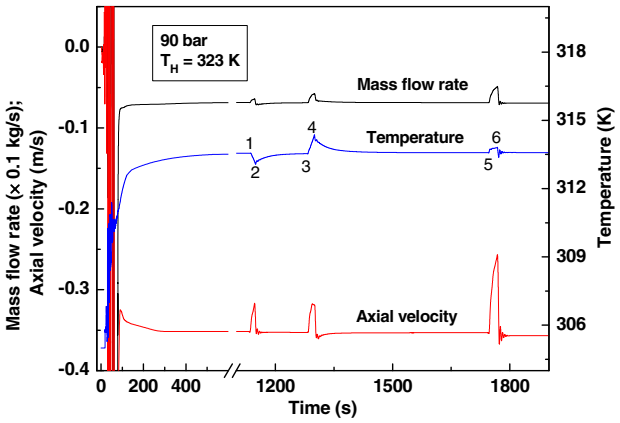

1- hot water pump off; 2- hot water pump on; 3- cold water pump off; 4- cold water pump on; 5- both pumps off, 6- both pumps on

Fig. 9. Effect of disturbances on loop stability at 90 bar.

and the experimental results is less than 7%, whereas it is less than 9% if compared with published numerical results, which could be termed as fairly reasonable.

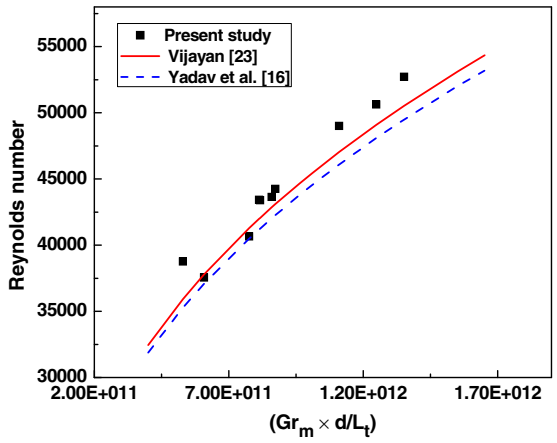

Fig. 10. Validation of simulation results with published data.

4. Conclusion

Transient, numerical simulation studies have been carried out on CO_2 based NCL at various operating conditions. Subcritical and supercritical phase of CO_2 are considered with operating pressure in the range of 50–100 bar and operating temperature in the range of 323 K to 363 K. Studies are carried out for various loop tilt angles, different initial conditions, and different water mass flow rates. Conclusions from the simulation results can be enumerated as:

(i) The loop fluid mass flow rate reaches a steady value earlier than temperature.
(ii) Heat transfer rate increases with increase in hot water inlet temperature due to greater temperature difference between CHX and HHX leading to higher buoyancy.
(iii) For stable flow, time to reach steady state decrease as operating pressure increases.
(iv) Results show that as tilt angle increases mass flow rate as well as heat transfer rate decrease. As the initial temperature of the loop increases, the system reaches steady state sooner.
(v) Flow start-up time and fluctuation in flow parameters for tilt in *YZ* plane is higher than those in *XY* plane.
(vi) Heat transfer rate and mass flow rate of CO_2 increase with increase in external water mass flow rate. Results show that the system reaches steady state faster at a higher mass flow rate of water which occurs due to the resulting higher heat transfer rate.
(vii) Stability of the loop was studied by turning off and turning on hot water and cold water pump. Results indicate the loop to be stable under the influence of all cases of disturbance applied.

Conflict of interest

None declared.

Acknowledgements

The study has been carried out under a project sponsored by Extramural Research Division, Council of Scientific and Industrial Research (CSIR), Government of India. The financial support provided by CSIR is gratefully acknowledged.

References

[1] K. Wang, E. Magnus, H. Yunho, R. Radermacher, Review of secondary loop refrigeration system, Int. J. Refrig. 33 (2010) 212–234.
[2] K. Kiran Kumar, M. Ram Gopal, Carbon dioxide as secondary fluid in natural circulation loops, Proc. IMechE Part E: J. Process Mech. Eng. 223 (2009) 189–194.
[3] A.K. Yadav, S. Bhattacharyya, M. Ram Gopal, On the suitability of carbon dioxide in forced circulation type secondary loops, Int. J. Low Carbon Technol. 9 (2014) 85–90.
[4] V. Dostal, P. Hejzlar, M.J. Driscoll, The supercritical carbon dioxide power cycle: comparison to other advanced power cycles, Nucl. Technol. 154 (2006) 283–301.
[5] P. Bondioli, C. Mariani, E. Mossa, A. Fedelli, A. Muller, Lampante olive oil refining with supercritical carbon dioxide, J. Am. Oil Chem. Soc. 69 (1992) 477–480.
[6] F.C.V.N. Fourie, C.E. Schwarz, J.H. Knoetze, Phase equilibria of alcohols in supercritical fluids. Part I: The effect of the position of the hydroxyl group for linear C8 alcohols in supercritical carbon dioxide, J. Supercrit. Fluids 47 (2008) 161–167.
[7] H. Yamaguchi, X.R. Zhang, K. Fujima, Basic study on new cryogenic refrigeration using CO_2 solid–gas two phase flow, Int. J. Refrig. 31 (2008) 404–410.
[8] K. Ochsner, Carbon dioxide heat pipe in conjunction with a ground source heat pump (GSHP), Appl. Therm. Eng. 28 (2008) 2077–2082.
[9] D.E. Kim, M.H. Kim, J.E. Cha, S.O. Kim, Numerical investigation on thermal-hydraulic performance of new printed circuit heat exchanger model, Nucl. Eng. Des. 238 (2008) 3269–3276.
[10] D.B. Kreitlow, G.M. Reistad, Themosyphon models for down hole heat exchanger application in shallow geothermal systems, J. Heat Transfer 100 (1978) 713–719.
[11] K.E. Torrance, Open-loop thermosyphons with geological application, J. Heat Transfer 100 (1979) 677–683.
[12] K. Kiran Kumar, M. Ram Gopal, Steady-state analysis of CO_2 based natural circulation loops with end heat exchangers, Appl. Therm. Eng. 29 (2009) 1893–1903.
[13] X. Zhang, L. Chen, H. Yamaguchi, Natural convective flow and heat transfer of supercritical CO_2 in a rectangular circulation loop, Int. J. Heat Mass Transfer 53 (2010) 4112–4122.
[14] L. Chen, X. Zhang, H. Yamaguchi, Z. (Simon) Liu, Effect of heat transfer on the instabilities and transitions of supercritical CO_2 flow in a natural circulation loop, Int. J. Heat Mass Transfer 53 (2010) 4101–4111.
[15] A.K. Yadav, M. Ram Gopal, S. Bhattacharyya, CFD analysis of a CO_2 based natural circulation loop with end heat exchangers, Appl. Therm. Eng. 36 (2012) 288–295.
[16] A.K. Yadav, M. Ram Gopal, S. Bhattacharyya, CO_2 based natural circulation loops: new correlations for friction and heat transfer, Int. J. Heat Mass Transfer 55 (2012) 4621–4630.
[17] B.E. Launder, D.B. Spalding, The numerical computation of turbulent flows, Comput. Methods Appl. Mech. Eng. 3 (1974) 269–289.
[18] J. Yang, Y. Oka, Y. Ishiwatari, J. Liu, J. Yoo, Numerical investigation of heat transfer in upward flow of supercritical water in circular tubes and tight fuel rod bundles, Nucl. Eng. Des. 237 (2007) 420–430.
[19] P.F. Lisboa, J. Fernandes, P.C. Simoes, J.P.B. Mota, E. Saatdjian, Computational-fluid-dynamics study of a Kenics static mixer as a heat exchanger for supercritical carbon dioxide, J. Supercrit. Fluids 55 (2010) 107–115.
[20] L. Chen, X.R. Zhang, Simulation of heat transfer and system behavior in a supercritical CO_2 based thermosyphon: effect of pipe diameter, ASME J. Heat Transfer 133 (2011) 122505 (8p).
[21] P.K. Vijayan, H. Austregesilo, Scaling laws for single-phase natural circulation loops, Nucl. Eng. Des. 152 (1994) 331–347.
[22] H.H. Bau, K.E. Torrance, Transient and steady behavior of an open, symmetrically heated, free convection loop, Int. J. Heat Mass Transfer 24 (1981) 597–609.
[23] P.K. Vijayan, Experimental observations on the general trends of the steady state and stability behaviour of single-phase natural circulation loops, Nucl. Eng. Des. 215 (2002) 139–152.
[24] S.K. Mousavian, M. Misale, F. D'Auria, M.A. Salehi, Transient and stability analysis in single-phase natural circulation, Ann. Nucl. Energy 31 (2004) 1177–1198.